Reconstruction method for curvilinear structures from two views

Matthias Hoffmann[a], Alexander Brost[c], Carolin Jakob[a], Martin Koch[a], Felix Bourier[d], Klaus Kurzidim[d], Joachim Hornegger[a,b], Norbert Strobel[e]

[a]Pattern Recognition Lab, Friedrich-Alexander-Universität Erlangen-Nürnberg, Erlangen, Germany
[b]Erlangen Graduate School in Advanced Optical Technologies (SAOT)
[c]Department of Radiology, Stanford University, Stanford, CA, USA
[d]Klinik für Herzrhythmusstörungen, Krankenhaus Barmherzige Brüder, Regensburg, Germany
[e]Siemens AG, Healthcare Sector, Forchheim, Germany

ABSTRACT

Minimally invasive interventions often involve tools of curvilinear shape like catheters and guide-wires. If the camera parameters of a fluoroscopic system or a stereoscopic endoscope are known, a 3-D reconstruction of corresponding points can be computed by triangulation. Manual identification of point correspondences is time consuming, but there exist methods that automatically select corresponding points along curvilinear structures. The focus here is on the evaluation of a recent published method for catheter reconstruction from two views. A previous evaluation of this method using clinical data yielded promising results. For that evaluation, however, no 3-D ground truth data was available such that the error could only be estimated using the forward-projection of the reconstruction. In this paper, we present a more extensive evaluation of this method based on both clinical and phantom data. For the evaluation using clinical images, 36 data sets and two different catheters were available. The mean error found when reconstructing both catheters was 0.1 mm ± 0.1 mm. To evaluate the error in 3-D, images of a phantom were acquired from 13 different angulations. For the phantom, A 3D C-arm CT voxel data set of the phantom was also available. A reconstruction error was calculated by comparing the triangulated 3D reconstruction result to the 3D voxel data set. The evaluation yielded an average error of 1.2 mm ± 1.2 mm for the circumferential mapping catheter and 1.3 mm ± 1.0 mm for the ablation catheter.

Keywords: Biplane, Fluoroscopy, Epipolar Geometry, Stereoscopy, Reconstruction, Catheter, Guide wire, Atrial fibrillation

1. INTRODUCTION

Atrial fibrillation is the most common heart arrhythmia and increases the risk of stroke significantly.[1] Cardiac ablation has become the standard treatment option for atrial fibrillation.[2] The ablation procedure is usually performed under fluoroscopic guidance using different catheters. In the fluoroscopic images, the catheters are clearly visible, whereas the left atrium, in which the ablation is performed, remains almost invisible due to the low soft tissue contrast of X-ray imaging unless contrast agent is administered. To add some soft-tissue information, an overlay image may be rendered from a pre-operatively acquired 3-D volume of the patient's heart and merged with the fluoroscopic images.[3] This overlay can be used to assess the position of the catheters with respect to anatomical structures of the heart.

For certain tasks during an electrophysiology (EP) procedure, 3-D catheter reconstruction would be beneficial. For example motion compensation of the overlay[4] or tracking[5,6] may require a 3-D reconstruction of a catheter. Moreover, reconstructions of catheters may provide a better orientation to the physician. Using a biplane X-ray system, a possible method for reconstruction is the manual annotation of corresponding points along the catheter in both images. Since this is very time consuming, a more automatic approach for reconstruction of curvilinear structures is favored.

Send correspondences to Matthias Hoffmann: Matthias.Hoffmann@cs.fau.de

Medical Imaging 2013: Image-Guided Procedures, Robotic Interventions, and Modeling, edited by David R. Holmes, Ziv R. Yaniv,
Proc. of SPIE Vol. 8671, 86712F (2013) doi:10.1117/12.2006346; http://dx.doi.org/10.1117/12.2006346

A first approach was presented by Baert *et al.*[6] It requires a 2-D curve for each image, which can be faster annotated than several pairs of corresponding points. As this approach shows problems with highly curved catheters, we presented an improved method[7] which is suited to reconstructing highly curved catheters. While the error in the first evaluation was measured only in 2-D for a single catheter type, we present a more comprehensive evaluation. We worked with two different catheter types and also computed the 3-D error of the reconstruction. The approach, however is not only limited to X-ray. A different application field is robotic surgery where imaging is done using stereoscopic endoscopes. If the camera parameters of the endoscope are known, this approach can be used for reconstruction of e.g. devices and vessels after segmentation.

This paper is structured as follows: Section 2 gives a detailed description of the reconstruction method, Section 3 describes the evaluation methods and the results of the evaluation and in Section 4, we discuss the results and draw conclusions.

2. METHODS

Reconstruction is performed based on two views A and B of a biplane system. For each plane, the projection matrix $\mathbf{P}_\mathrm{A}$ and $\mathbf{P}_\mathrm{B} \in \mathbb{R}^{3\times4}$, respectively, and a 2-D curve that models the catheter is required as input. These curves, $C_\mathrm{A}(t_\mathrm{A})$ and $C_\mathrm{B}(t_\mathrm{B})$, $t_\mathrm{A}, t_\mathrm{B} \in [0,1]$ are usually provided as cubic spline curves. It is not required that the curves share the same start- and endpoint, the direction, however, has to be the same. The reconstruction approach can be divided into three parts: First, possible point correspondences are determined. Second, a set of point correspondences is selected and third, the 3-D curve is reconstructed using these point correspondences. The computation uses homogeneous coordinates. Given a 2-D point $\mathbf{h}$, $\tilde{\mathbf{h}}$ denotes the homogeneous extension of $\mathbf{h}$. In the first step, the fundamental matrix $\mathbf{F}_\mathrm{A} \in \mathbb{R}^{3\times3}$ needs to be determined. Using the projection matrices $\mathbf{P}_\mathrm{A}$ and $\mathbf{P}_\mathrm{B}$, it can be computed by[8]

$$\mathbf{F}_\mathrm{A} = [\mathbf{P}_\mathrm{B} \cdot \tilde{\mathbf{o}}_\mathrm{A}]_\times \mathbf{P}_\mathrm{B} \mathbf{P}_\mathrm{A}^\dagger \ . \tag{1}$$

Here, the cross-product is expressed in terms of a skew matrix

$$[\mathbf{c}]_\times = \begin{pmatrix} 0 & -c_3 & c_2 \\ c_3 & 0 & -c_1 \\ -c_2 & c_1 & 0 \end{pmatrix} . \tag{2}$$

The camera center $\tilde{\mathbf{o}}_\mathrm{A} \in \mathbb{R}^4$ of plane A can be computed as the nullspace of $\mathbf{P}_\mathrm{A}$, $\mathbf{P}_\mathrm{A}^\dagger$ denotes the pseudo-inverse[9] of $\mathbf{P}_\mathrm{A}$. For computing all possible point correspondences, a sequence of n points $\mathbf{a}_1 \dots \mathbf{a}_n$ is acquired by sampling the curve C_A equidistantly from the start to the end. The spline parameter of the i-th sample point is denoted by t_i. For every sampled point $\mathbf{a}_i$ the epipolar line $\mathbf{l}_i \in \mathbb{R}^3$ is computed by

$$\mathbf{l}_i = \mathbf{F}_\mathrm{A} \tilde{\mathbf{a}}_i \ . \tag{3}$$

As all points in B corresponding to $\mathbf{a}_i$ have to lie on $\mathbf{l}_i$, the set of possible corresponding points $\mathbf{b}_{i,1} \dots \mathbf{b}_{i,m}$ in B is computed by intersecting the curve in B with $\mathbf{l}_i$, see Figure 1(b). The intersections are saved as correspondence pairs $(t_i, t_{i,1}) \dots (t_i, t_{i,m})$ with $C_\mathrm{A}(t_i) = \mathbf{a}_i, C_\mathrm{B}(t_{i,j}) = \mathbf{b}_{i,j}$.

The goal of the second step is to create a correspondence function $f : t_\mathrm{A} \to t_\mathrm{B}$ that maps a point $C_\mathrm{A}(t_\mathrm{A})$ of the curve in plane A to a point $C_\mathrm{B}(t_\mathrm{B})$ of the curve in plane B. The control points of f will be a subset of the correspondence pairs which were computed in the first step as shown in Figure 1(c). Once f is established, point correspondences for arbitrary points $C_\mathrm{A}(t_\mathrm{A})$ can be computed by interpolating between the control points of f. Since both curves follow the same direction, f has to be monotonous. This implies that if for a point $\mathbf{a}_j$ the point $\mathbf{b}_{j,k}$ is selected as corresponding point, then for the point $\mathbf{a}_{j+1}$ a point $\mathbf{b}_{j+1,l}$ must not be selected if it is located *before* $\mathbf{b}_{j,k}$, i.e. if $t_{j+1,l} < t_{j,k}$.

The subset containing the most correspondence pairs satisfying this constraint will be referred as the *optimal set* which defines the *optimal correspondence function*. This set can be computed greedily[6] by sampling points along C_A and selecting as corresponding point to $\mathbf{a}_i$ the point $\mathbf{b}_{i,j}$ which comes directly after the previous selected corresponding point. This is the point which has the smallest parameter $t_{i,j}$ that is still greater than all parameters t_B of previously included pairs (t_A, t_B), $t_\mathrm{A} < t_i$. This method, however, can lead to wrong results in

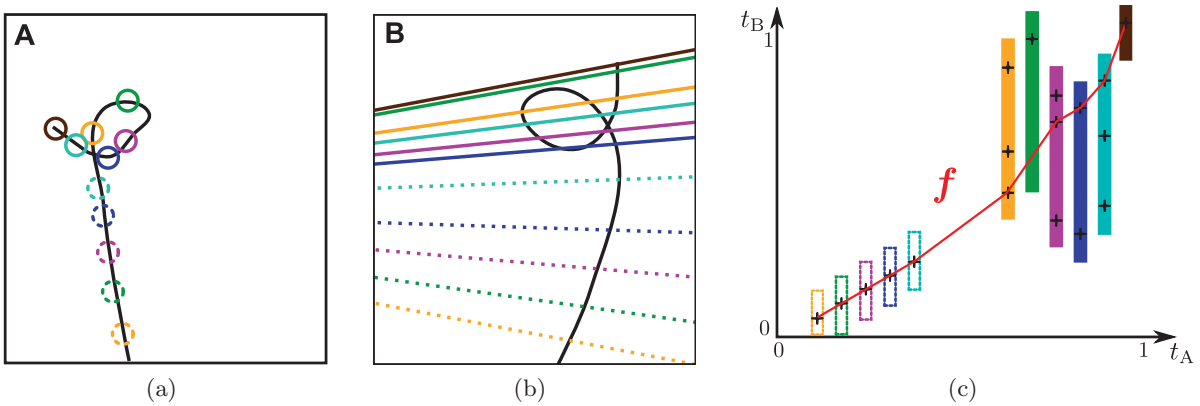

Figure 1. For reconstruction, points of the curve in (a) are sampled. For each point, the corresponding epipolar line is computed and the intersections with the curve in (b) are computed. These intersection points are stored (c) and a correspondence function is fitted through them. This function maps the first curve to the second curve. It is monotonic and includes as many intersection points as possible. Due to inaccuracies in a practical setup, the epipolar line might not intersect the curve in (b) at the actual corresponding point as demonstrated by the solid green line. These missing point correspondences can be interpolated using the correspondence function.

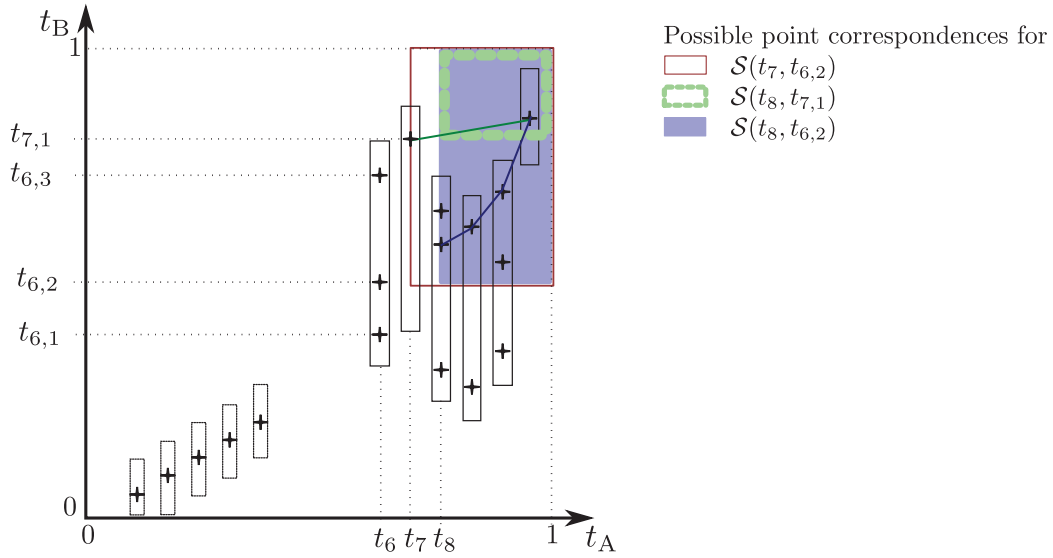

Figure 2. To compute $\mathcal{S}(t_7, t_{6,2})$ one could include the point correspondence $(t_7, t_{7,1})$ and add it to the $\mathcal{S}$ of the green area. This would result in the correspondences on the green line. Another posibility is to ignore the correspondences from t_7 and take the $\mathcal{S}$ which includes point correspondences from the green area. This $\mathcal{S}$, which includes the correspondence pairs on the blue line, will be choosen by the algorithm since it is the larger one

a practical setup: The epipolar line of a point $\mathbf{a}_i$ might ideally intersect C_B at two points $\mathbf{b}_{i,1}$ and $\mathbf{b}_{i,2}$ with $\mathbf{b}_{i,1}$ being the true corresponding point of $\mathbf{a}_i$. If, due to inaccuracies, the first intersection is not found, $\mathbf{b}_{i,2}$ would be mistakenly selected as corresponding point. For following points in A, the correct corresponding points in B cannot be selected if they are located before the mistakenly chosen point $\mathbf{b}_{i,2}$. This scenario happens often for highly curved objects where the epipolar line is tangential to the object, like the solid green line in Figure 1(b). In this case a small deviation causes the epipolar line to miss the curve and no intersection point will be found at this position.

To overcome this issue, we search for the optimal set once all possible point correspondences have been computed. Computing the optimal set can be expressed by a recursive formulation. $\mathcal{S}(t_i, t_B)$ denotes the optimal set of point correspondences when considering the subcurves from $C_A(t_i)$ and $C_B(t_B)$ to the end. Figure 2 shows

Table 1. Acquisition angles of the phantom data.

Sequence number	1	2	3	4	5	6	7	8	9	10	11	12	13
Plane A	-30	-20	0	10	30	-30	-20	-20	-50	-40	-30	55	52
Plane B	-120	-110	-90	-80	-60	-110	-100	-90	-120	-110	-100	-67	-77
Angular difference	90	90	90	90	90	80	80	70	70	70	70	122	129

The primary angle in degree is given for each sequence and image plane as well as the angular difference in degree between both C-arms. The secondary angle is set to 0° for all sequences.

the reduced set of point correspondences. Assuming n sampled points of the curve C_A, the base case of the recursion is

$$\mathcal{S}(t_{n+1}, 1) = \{\} \tag{4}$$

as there are no correspondences after the end of the curve. $\mathcal{S}(t_1, 0)$ yields the optimal set for the whole curves. For computing the set $\mathcal{S}(t_i, t_\mathrm{B})$, we take the intersections of C_B and the epipolar line corresponding to $\mathbf{a}_i$. The correspondence function is monotonic and we do not want to deprive us of including subsequent intersection points by proceeding too far along C_B. Therefore, we consider the intersection point $(t_i, t_{i,j})$ with the lowest value $t_{i,j}$ that is still larger than t_B. The j for which this applies is denoted as

$$\hat{j} = \min(j),\ t_{i,j} \geq t_\mathrm{B}\ . \tag{5}$$

There are two choices: First, we could decide for this point correspondence $(t_i, t_{i,\hat{j}})$ and return it together with the optimal set $\mathcal{S}(t_{i+1}, t_{i,\hat{j}})$ of the remaining curves. The subcurves start at $C_\mathrm{A}(t_{i+1})$ and $C_\mathrm{B}(t_{i,\hat{j}})$ and the parameters of $\mathcal{S}$ are therefore set accordingly. The second possibility is to ignore this point and to proceed only along curve C_A. This might be necessary if the epipolar line does not intersect C_B at the true corresponding point as demonstrated by the solid green line in Figure 1(b). The optimal set $\mathcal{S}(t_{i+1}, t_\mathrm{B})$ of the remaining subcurve is returned. As we do not proceed in C_B, the second parameter remains unchanged.

Since the optimal set is defined as the set holding the most correspondences, we decide for that posibility which returns the larger set:

$$\mathcal{S}(t_i, t_\mathrm{B}) = \begin{cases} \{\} & \text{if } t_i > 1 \text{ or } t_\mathrm{B} > 1 \text{ (base case)} \\ (t_i, t_{i,\hat{j}}) \cup \mathcal{S}(t_{i+1}, t_{i,\hat{j}}) & \text{if } 1 + |\mathcal{S}(t_{i+1}, t_{i,\hat{j}})| > |\mathcal{S}(t_{i+1}, t_\mathrm{B})| \\ \mathcal{S}(t_{i+1}, t_\mathrm{B}) & \text{else} \end{cases} \tag{6}$$

In practice, $\mathcal{S}$ is computed by dynamic programming.[10] In the third step, the point correspondences of the optimal set are used to reconstruct 3-D points according to Brost et al.[11]

3. EVALUATION AND RESULTS

Evaluation of the reconstruction was carried out both with clinical data and images of a phantom. The evaluation using clinical data involved 36 biplane images from 28 cases each depicting a circumferential mapping catheter. We also evaluated ablation catheter reconstruction based on 36 biplane images from 18 cases. The catheters depicted in the clinical images were marked by a physician and used as input for the reconstruction. As no 3-D data were available, the resulting 3-D catheter reconstruction was forward projected into the planes and the difference between the input and the projection was computed. The overall mean error for the circumferential mapping catheter is 0.1 mm ± 0.1 mm. The maximum error is 1.2 mm. The error for each biplane pair is given in Figure 3. For the ablation catheter, the mean error is 0.1 mm ± 0.1 mm, the maximum error is 0.2 mm. Figure 4 shows the error for each biplane pair. An example of a reconstruction is given in Figure 6.

The error in 3-D was evaluated using phantom experiments. To this end, a scene comprising a circumferential mapping catheter and an ablation catheter was prepared and tomographically reconstructed using C-arm CT. Then 13 biplane images of the scene were taken, each at a different angulation. The primary angles of the C-arm are given in Table 1, the secondary angle was kept fixed at 0°. The 3-D position of the circumferential mapping catheter was extracted out of the C-arm CT data and compared with the reconstruction results using the biplane

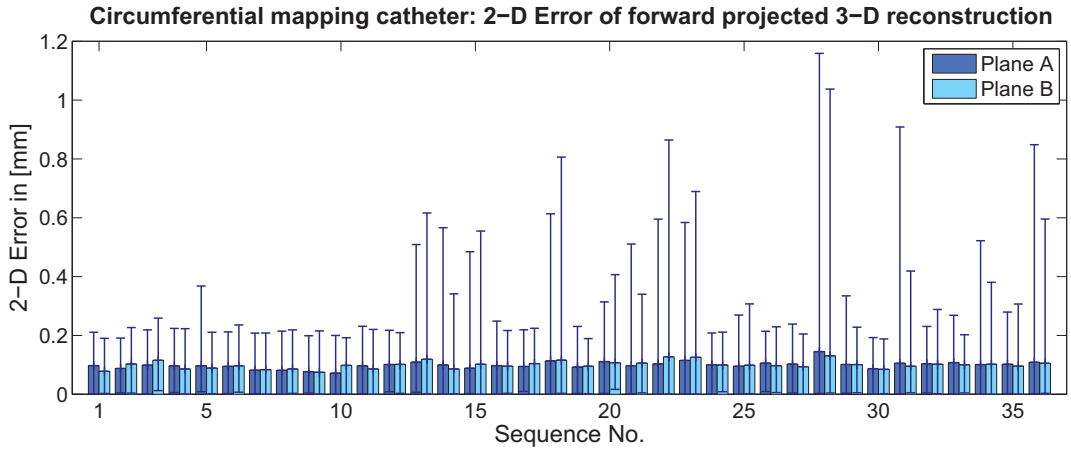

Figure 3. Difference between the reprojection of the reconstruction and the gold standard for the circumferential mapping catheter. The thin bars denote the minimal and maximal error. The overall mean error is 0.1 mm ± 0.1 mm, the overall maximum error is 1.2 mm.

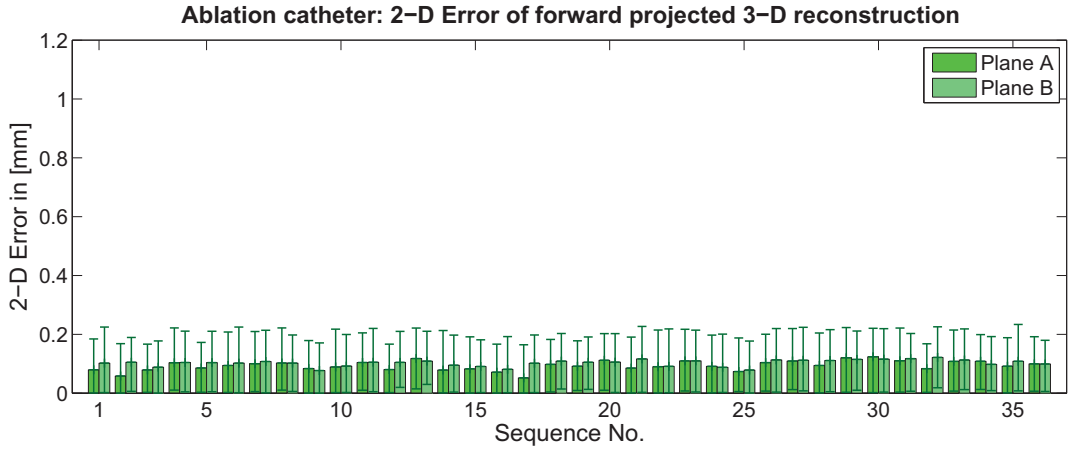

Figure 4. Difference between the reprojection of the reconstruction and the gold standard for the ablation catheter. The thin bars denote the minimal and maximal error. The overall mean error is 0.1 mm ± 0.1 mm, the overall maximal error is 0.2 mm.

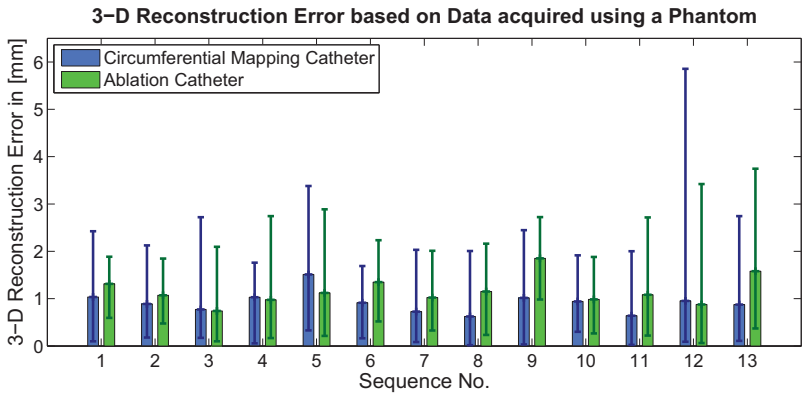

Figure 5. Mean reconstruction errors for each sequence, the thin bars denote the maximal and minimal error. The total mean error is 1.2 mm ± 1.2 mm for the circumferential mapping catheter and 1.3 mm ± 1.0 mm for the ablation catheter.

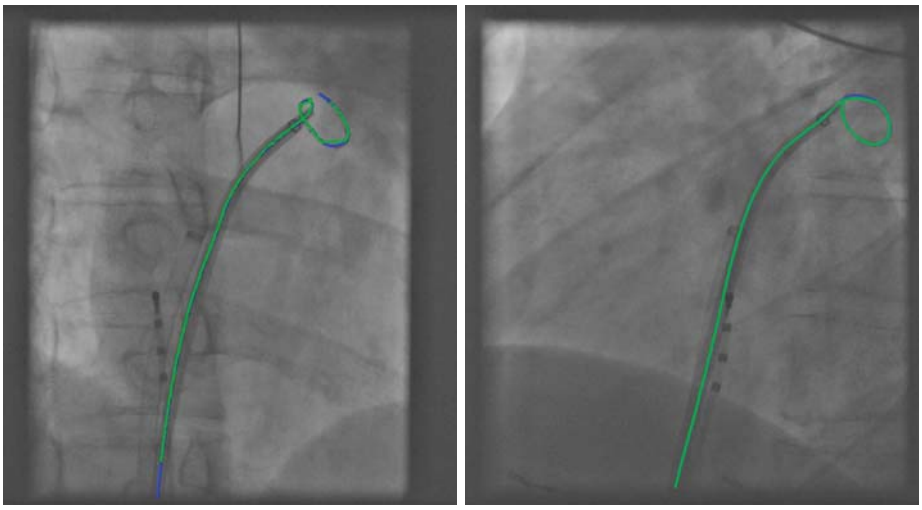

(a) Image plane A (b) Image plane B

Figure 6. Reconstruction result of a circumferential mapping catheter. The blue line denotes the gold-standard annotation, the green line shows the projection of the reconstruction. This biplane pair corresponds to sequence No. 28 in Figure 3.

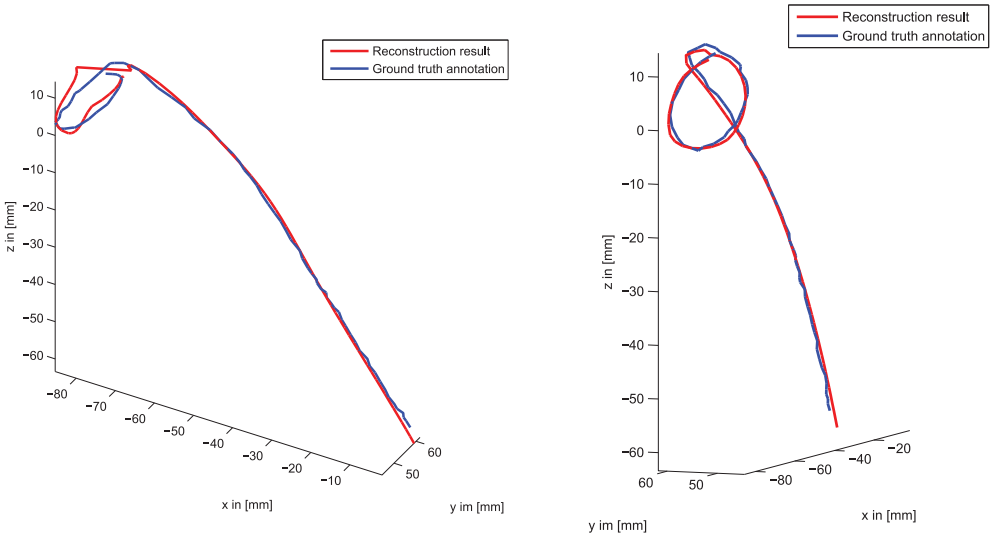

Figure 7. Reconstruction result of a circumferential mapping catheter from two different views. The blue line denotes the gold-standard annotation, the red line shows the reconstruction result. This biplane pair corresponds to sequence No. 12 in Figure 5.

images. The outcomes are presented in Figure 5. The mean error over all sequences is 1.2 mm ± 1.2 mm for the circumferential mapping catheter and 1.3 mm ± 1.0 mm for the ablation catheter. The maximal error is 5.8 mm for the circumferential mapping catheter and 3.7 mm for the ablation catheter. The reconstruction result with the highest maximal error is shown in Figure 7

The evaluation was computed on an Intel i7 with 2,67 GHz and 4 GB RAM and required on average 0.15 s which corresponds to a frame rate of 6 frames per second.

4. DISCUSSION AND CONCLUSIONS

Thanks to improvements in calibration techniques, the error of the reprojection could be reduced compared to our previous evaluation.[7] With a mean error of 0.1 mm it is in the range of the pixel spacing of the detector which

was 0.1725 mm. When comparing the maximum error of the circumferential mapping catheter and the ablation catheter, the error for the circumferential mapping catheter is much higher. Although the point correspondences were selected in an optimal way, the reconstruction of highly curved objects is still more error prone compared to straight objects such as the ablation catheter. Figure 6 shows that errors occurred at the bottom and the top of the elliptical catheter tip. Due to the camera setup, the main direction of the epipolar lines is horizontal. So, these are the points where the epipolar line is tangent to the catheter and touches it in a single point. Minor inaccuracies can lead to a small displacement resulting in a missed intersection point. The missing point correspondences are interpolated using the optimal correspondence function which still leads to a satisfying result.

The evaluation of the 3-D error reveals higher values compared to the reprojected 2-D error which compares the reconstruction result with the input of the algorithm. Therefore, errors in the annotation of the catheter play only a minor role. The 3-D error, however, receives as input the annotation in 2-D and compares the reconstruction result to the 3-D annotation. Inconsistencies in the annotations for the A-plane, the B-plane and the 3-D data, respectively, could be one reason for the higher 3-D error. Moreover, the 2-D errors in both images may combine to a higher 3-D error. However, the error is still small enough to justify using our approach in a clinical environment.[12]

Disclaimer

The concepts and information presented in this paper are based on research and are not commercially available.

Acknowledgements

This work was supported by the German Federal Ministry of Education and Research (BMBF) in the context of the initiative Spitzencluster Medical Valley - Europäische Metropolregion Nürnberg, project grant Nos. 01EX1012A and 01EX1012E, respectively. Additional funding was provided by Siemens AG, Healthcare Sector.

REFERENCES

[1] Wolf, P., Abbott, R., and Kannel, W., "Atrial fibrillation as an independent risk factor for stroke: the Framingham study," *Stroke* **22**(8), 983–988 (1991).

[2] Calkins, H., Brugada, J., Packer, D., Cappato, R., Chen, S., Crijns, H., Damiano, R., Davies, D., Haines, D., Haissaguerre, M., et al., "HRS/EHRA/ECAS expert consensus statement on catheter and surgical ablation of atrial fibrillation: recommendations for personnel, policy, procedures and follow-up," *Europace* **9**(6), 335 (2007).

[3] Bourier, F., Vukajlovic, D., Brost, A., Hornegger, J., Strobel, N., and Kurzidim, K., "Pulmonary vein isolation supported by MRI-derived 3D-augmented biplane fluoroscopy: A feasibility study and a quantitative analysis of the accuracy of the technique," *Journal of Cardiovascular Electrophysiology* (2012).

[4] Brost, A., Liao, R., Strobel, N., and Hornegger, J., "Respiratory motion compensation by model-based catheter tracking during ep procedures," *Medical Image Analysis* **14**(5), 695–706 (2010).

[5] Schenderlein, M., Stierlin, S., Manzke, R., Rasche, V., and Dietmayer, K., "Catheter tracking in asynchronous biplane fluoroscopy images by 3d b-snakes," in [*Medical Imaging 2010: Visualization, Image-Guided Proceudres, and Modeling*], Wong, K. and Miga, M., eds., *Proceedings of SPIE* **7625**, 76251U1–76251U9 (February 13th – 18th 2010).

[6] Baert, S., van de Kraats, E., van Walsum, T., Viergever, M., and Niessen, W., "Three-dimensional guide-wire reconstruction from biplane image sequences for integrated display in 3-d vasculature," *IEEE Transactions on Medical Imaging* **22**(10), 1252–1258 (2003).

[7] Hoffmann, M., Brost, A., Jakob, C., Bourier, F., Koch, M., Kurzidim, K., Hornegger, J., and Strobel, N., "Semi-automatic Catheter Reconstruction from Two Views," in [*Medical Image Computing and Computer-Assisted Intervention – MICCAI 2012*], Ayache, N., Delingette, H., Golland, P., and Mori, K., eds., *Lecture Notes in Computer Science* **7511**, 584–591, Springer (2012).

[8] Hartley, R. and Zissermann, A., [*Multiple view geometry in computer vision*], Cambridge Univ Press (2010).

[9] Golub, G. and Kahan, W., "Calculating the singular values and pseudo-inverse of a matrix," *Journal of the Society for Industrial and Applied Mathematics: Series B, Numerical Analysis* **2**, 205–224 (1965).

[10] Cormen, T., Leiserson, C., and Rivest, R., [*Introduction to algorithms*], MIT Press (1990).

[11] Brost, A., Strobel, N., Yatziv, L., Gilson, W., Meyer, B., Hornegger, J., Lewin, J., and Wacker, F., "Geometric Accuracy of 3-D X-Ray Image-Based Localization from Two C-Arm Views," in [*Workshop on Geometric Accuracy In Image Guided Interventions-Medical Image Computing and Computer Assisted Interventions, MICCAI*], Yang, G.-Z., Hawkes, D., Rueckert, D., Noble, A., and Taylor, C., eds., 12–19 (September 20th – 24th 2009).

[12] Esteghamatian, M., Azimifar, Z., Radau, P., and Wright, G., "Real-time 2D-3D MR cardiac image registration during respiration using extended Kalman filter predictors," in [*9th International Conference on Signal Processing, 2008*], 1325–1328, IEEE (May 10th – 11th 2008).